Composite Structures xxx (2020) 113226

Contents lists available at ScienceDirect

Composite Structures

journal homepage: www.elsevier.com/locate/compstruct

Reserach

Predication of the in-plane mechanical properties of continuous carbon fibre reinforced 3D printed polymer composites using classical laminated-plate theory

Khalid Saeed *, Alistair McIlhagger, Eileen Harkin-Jones, John Kelly, Edward Archer

Engineering Research Institute, Ulster University, Jordanstown, Newtownabbey, Co. Antrim BT37 0QB, United Kingdom

ARTICLE INFO

Keywords:
Additive manufacturing (AM)
Continuous carbon fibre polymer composites (CCFPC)
Fused deposition modelling (FDM)

ABSTRACT

In this study in-plane mechanical properties of continuous carbon fibre reinforced thermoplastic polyamide composite manufactured using a Markforged Two 3D printing system was evaluated and compared against predicted values from classical laminated-plate theory. Strength, stiffness and Poisson's ratio of the composite specimens were measured using tensile testing both in longitudinal and transverse direction and the shear properties were also measured. The influence of fibre orientation on mechanical properties was investigated and were compared with that of non-reinforced nylon samples and known material property values from literature. It was determined that the modulus of elasticity and tensile strength values were significantly improved to 603.43 MPa and 85 GPa respectively as compare to unreinforced nylon specimens. Furthermore, cross-sectional micrographs of specimens are analysed to observe the microstructure and fracture mechanism of the 3D printed composite. Experimentally determined values were used to predict the behaviour of the materials in different orientation using classical laminated-plate theory on the commercially available LAP (Laminated Analysis programme) software. The model developed will allow the designers to predict the elastic (mechanical) properties of 3D printed parts reinforced with fibre for components which require specific mechanical properties.

1. Introduction

Additive Manufacturing (AM) technologies also known as 3D printing (Rapid Prototyping), is a technique of making physical/solid objects by depositing one layer upon the other layer sequentially as opposed to subtractive manufacturing methodologies to achieve the desire properties [1]. Objects are fabricated and different properties like mechanical, thermal, optical, electrical are measured if it is suitable for specific applications. Parts are design in 3D computer aided design (CAD) software's before importing to the printer in surface tessellation language (STL) format. 3D printing technology is used in several areas including aerospace, automobiles, defence and medical industry [2,3]. 3D printing in medical field can be used to develop artificial scalp, implants, prosthetics hand and crynostpics [4]. Raw data can be obtained using computerized tomography (CT) scan and Magnetic resonance imaging (MRI) to create a 3D file which are then feed for the printing machine which are then post process to achieve better accuracy and surface finish [5]. AM techniques are normally used for fabricating pure thermoplastic 3D prototypes but not limited only to polymers. Various AM techniques have been developed including Stereolithography (SLA), Selective laser sintering (SLS), Laminated object manufacturing (LOM), Fused deposition modelling (FDM).

Fused deposition modelling (FDM) is one of the promising AM techniques widely used to manufacture complex and intricate structures using material in filament form due to its relative low cost, low materials wastage, flexible material changes and consistent accuracy [6]. It is a solid-based AM process, in which semi-finished filaments are extruded by a driving gear and a grooved bearing. The feedstock materials would be extruded at a constant nozzle temperature and are deposited on to the print bed according to tool path generated by the slicing software; thereafter the print bed platform moves downward by a layer thickness for subsequent layer deposition until the part is completed. Parts produced by FDM does not require any post processing as most of the other 3D printing techniques do and can be handled straight away after cooling. Polyamide/Nylon (PA), Polylactic acid (PLA), Acrylonitrile Butadiene Styrene (ABS) and polycarbonate

* Corresponding author.
E-mail addresses: Saeed-k@ulster.ac.uk (K. Saeed), a.mcilhagger@ulster.ac.uk (A. McIlhagger), e.harkin-jones@ulster.ac.uk (E. Harkin-Jones), j.kelly@ulster.ac.uk (J. Kelly), e.archer@ulster.ac.uk (E. Archer).

https://doi.org/10.1016/j.compstruct.2020.113226
Received 31 July 2020; Accepted 1 November 2020
Available online xxxx

(PC) are the typical thermoplastic materials that are processed through FDM [7,8]. Since the parts built using pure thermoplastic by FDM lacks strength and stiffness as fully load bearing. One of the possible methods is the addition of reinforced materials into plastic material to form a thermoplastic polymer composite. Introducing carbon fibre into polymer can improve the strength and stiffness of the 3D printed parts enabling it for high value applications.

FDM 3D printing of polymer composites can be categorized in two groups: 1) short fibre reinforced thermo plastic (SFRT) and 2) continuous fibre reinforced thermoplastic (CFRT) composite. Currently, short carbon fibre reinforced polymer composites are extensively produced using AM, but it has shown limited improvements in mechanical properties in certain direction as the orientation and alignment of the short carbon are difficult to control. Continuous fibre reinforcement composite is an FDM based AM technique becomes an alternative manufacturing technique due to excellent mechanical properties, recycling, and potential uses in light weight structure. Currently, polymer composites are mainly used fuselage of Airbus A350 aircraft, components in automotive, blades of wind turbine, and endoscopy surgery equipment [9].

Yong et al. [10] studied the synergetic reinforcement effect of both short and continuous carbon fibres on the mechanical properties of 3D printed polymer based composites. The results showed that the synergetic reinforcement of laminated composites by both short and continuous carbon fibre was indeed superior to the individual carbon fibre reinforcement for the tensile strength but not for the elastic modulus. Another study by F. Ning et al. [11], studied the effects of process parameters such as nozzle temperature, infill speed, raster angle, layer thickness on tensile properties of carbon fibre reinforced polymer composites using fused deposition modelling. Tensile strength, Young's modulus, and yield strength had the largest mean values with a layer thickness of 0.15 mm because the coalesced interlayers generated a great inter bonding strength. However, the findings this study indicate a limited improvement of mechanical properties which is still below the actual requirements in engineering applications. In another research by Goh et al. [12] characterized carbon and glass fibre reinforced thermoplastic fabricated parts by FDM technique using tensile, flexural and indentation tests and compared with conventional composite manufacturing processes. Additionally, similar fracture behaviour was observed for tensile and quasi-static indentation tests.

Tekinalp et al. [1] revealed from the Microstructure-Mechanical property relationship that a relative high porosity of about 20% is observed in 3D printed composites as compared to the parts fabricated through compression moulding, yet both exhibits comparable strength and modulus. The difference in strength between the two types of fibre reinforced samples was minor, with fibre alignment from 0 to 90° in FDM samples, versus the random orientation of the fibre in samples prepared through compression moulding, compensating for some of the strength loss from porosity. Strength and stiffness of the 3D printed parts as lower as compared to other conventional manufacturing techniques due to lower amount of fibre contents as the fibre volume fraction was reported to be 34.5% by Van Der Klift [13].

In this work, mechanical properties and microstructure analysis of continuous carbon fibre reinforced 3D printed specimens are investigated. Carbon fibre are known for their high stiffness to weight ratio but expensive ($150 per 50 cm^3) as compare to glass fibre ($100 per 50 cm^3) and consequently are used only in industries that are very cautious about weight such as aerospace industry. To understand the structure and distribution of the fibre and the filament microstructural microscopy were carried out. Analytical analysis of the 3D printed parts was utilized to understand and subsequently predict the failure load and mode respectively. One of the aims of this paper is to determine the mechanical properties of polymer composites 3D printed parts so that they can be utilized for the computer modelling applications. Successful determination of the mechanical properties needed for an analytical analysis of a 3D printed part will need an FDM printer to print several test pieces under different printing conditions followed by tensile testing using angle minus longitudinal (AML) technique. Analytical approach using LAP will be adopted to figure out the optimum alignment of fibre and this will be validated using classical laminated theory (CLT) [14].

This paper is structured as follows; first materials used, specimen fabrication, testing parameters, testing and measurement is discussed along with the analysis of the test data. Thereafter, tensile test data are summarized and are compared with the data available in the literature. Material constants were extracted from the experimental data at different fibre angle orientation and were used for LAP analysis. Finally, conclusion was drawn based on experimental data, prediction of the material constants for different AML and the limitations of the process.

2. Experimental methods

2.1. Materials and processing

Mark forged Two printer was used to developed 3D printed parts using basic FDM principles [15]. Mark forged Two printer has dual extrusion nozzles provides the ability to print thermoplastic (Nylon) polymer followed by a fibre (Carbon, glass, Kevlar) reinforced to form a polymer composite matrix having light weight with enhanced properties. The nozzle diameter of the nylon filament is 0.4 mm, almost the same as conventional plastic filament 3D printers. Shape of fibre nozzle is smooth, and it may be deigned to prevent abrasion between the fibres and the metallic nozzle.

Nylon was used as the effective matrix filament and was supplied by Goprint3d, UK a supplier of Markforged, Cambridge, MA, USA. It is the proprietary blend of Markforged, and has a diameter of 1.75 mm. Prior, to printing it was stored in a moisture-sealed Markforged Nylon dry box (Pelican case) to prevent deterioration of the filament due to moisture abortion during the storage and a pack of silica gel desiccant was placed in the dry box in order to avoid moisture absorption. The reinforcing carbon fibre (CF) was also supplied by Goprint3d having a diameter of 0.35 mm impregnated with a sizing agent. Chemical composition and the mechanical properties of the neat fibres were withheld by the supplier. Differential scanning calorimetry (DSC), thermo gravimetric analysis (TGA) techniques were used to characterize and to find the melting, transition and decomposition temperature.

2.2. Specimen 3D printing (fabrication)

All the specimen including reinforced and unreinforced were fabricated using Mark forged Two desktop 3D printer. The reinforced samples consist of a core of a continuous fibre and Nylon at the outer layers in a smaller amount. A minimum of at least two layers of Nylon are required at the top and bottom of all printed parts as imposed by the closed source slicing software (Eiger). This may help in removing the part from the print bed easily and to avoid exposing the fibre to the outer surface to achieve better surface finish with the Nylon. By printing the top, bottom and side walls of Nylon has a negative impact as it lowers the amount fibre reinforcement and in turn reduce the possibility of achieving maximum mechanical properties. The orientation of the fibers can be controlled through the Eiger software on a layer by layer basis. The process parameters such as printing (infill) speed, nozzle temperatures and layer thickness were automatically set by the printer slicing software according to the material selection and the thickness of the layer. The infill percentage selected for printing all the specimen was kept at 100% (solid fill) which are summarized in Table 1. Deposition positioning for printing with Nylon was automatically set by the Eiger as ±45° alternatively for nylon specimens while for composite specimen only first and last layer was of nylon as shown

in Fig. 1. Infill pattern selected for fibre reinforced specimens was isotropic, strength, stiffness and failure mode changes by changing the infill type. Fibre volume fraction estimation is also critical and is reported to 35% using characterization techniques [16,17].

The mark forged Two 3D printer do not have any heating mechanism for the print bed (build platform). The compaction pressure is not a directly controlled process parameter, as it is related to the gap between the build platform and printer nozzle. The bed levelling was kept the same for all the specimens. During printing of the unidirectional specimens, starting point of each layer was the same as opposed to ±45 specimens in which starting point changes after every layer deposition (Fig. 2).

2.3. Testing parameters

Performance of fibre reinforced specimens were evaluated by conducting tensile testing with a pre strain load of 2 N in the clamps prior to start the test. The test setup used to evaluate the stress strain behavior of 3D printed specimens is shown in Fig. 3. Tensile tests were carried out using MTS with a 100 KN load cell to apply load to the test specimen. Two extensometers were used to measure the strain both in longitudinal and transverse direction. Strain of the test samples was measured using a 25.4 mm gauge length extensometer (Model number 634.11F-5x) in longitudinal direction. Specimens were tested at a strain rate of 2 mm/min. To make sure of the better accuracy of the test results, five samples of each type were tested. Poison's ratio was determined by measuring the strain in longitudinal and transverse direction.

2.4. Testing and measurement

Initially the ASTM D638 standard procedure was followed using Type 1 dog bone shape geometry [18]. However, the failure of the tensile samples in undesired area as described by Forster [19] required the adoption of the ASTM D3039 procedure that are specifically designed for polymer composites. The dimension of the samples used was 165 mm × 19 mm × 3.2 mm according to ASTM D3039 standard. Primarily samples were printed and tested using the tensile machine, but the fracture location in the samples were not in the gage length. Glass tabs were then bonded at the ends of the test samples with Araldite 2014 two-part adhesive to diminish the effect of stress concentration produced due to the griping of the sample in the machine. Samples ends were abraded to remove the nylon layer as the bonding was not perfect and slippage occur without removing the nylon layer. The glass tabs having a dimension of 25 mm × 19 mm were then bonded using Araldite adhesive using pressure for 24 h.

2.5. Mechanical test results

Samples manufactured of nylon were tested first for reference purpose. Stress verses strain curves were obtained from the data and the values for Young's modulus, Poisons ratio and other parameters were obtained from the experimental data and are summarized in Table 2. Tensile test for the unreinforced samples made of Nylon and Onyx were tested to compare with the manufacturer values and to evaluate the effect of fibre contents on the mechanical properties of the composite specimens. Mean values for five samples of Nylon and Onyx samples are summarized in Table 1. Tensile strength at yield σ_y and tensile strength at break σ_u was calculated using $\sigma_y = \frac{F_{max}}{A_o}$ and $\sigma_u = \frac{F_{break}}{A_o}$ relations respectively. Elastic modulus and yield strength of 780 MPa and 31.19 MPa was recorded as it the same values as observed by Biron [20].

Table 1
FDM printing parameters for tensile 3D printed composite samples.

Parameters	Specifications
Fibre fill type	Isotropic
Fill density	100%
Fibre layers	24
External layers	1
No. of top layers	1
No. of bottom layers	1
Concentric fibre rings	0
Fibre orientation (angle)	0, ±45, 90, Quasi-isotropic (0, ±45,90)

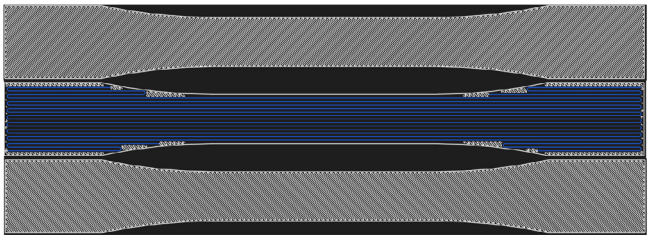

Fig. 1. Printing configuration (fibre in longitudinal direction) in Eiger for composite specimens.

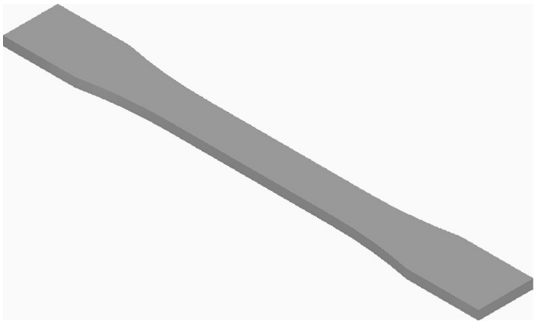

Fig. 2. Sample geometry designed in computer aided design software (Solid edge) before importing to the slicing software.

Fig. 3. Sample tensile testing set up with extensometers in longitudinal and transverse direction to measure strain.

Table 2
Improvements in properties of Nylon and Onyx in comparison to the manufacturer datasheet.

Material	Elastic Modulus (MPa)	Tensile strength (MPa)	Yield strength (MPa)	Poison 's ratio (υ)	Strain at failure (%)
Nylon	780	58.76	31.19	0.40	548.32
Manufacturer	940	54	31	–	260
Onyx	950	37.83	34.32	0.38	45
Manufacturer	1400	30	36	–	58

It is known that the parts produced using 3D printing technologies results in anisotropic properties in the three major coordinates axes. The anisotropy becomes significant for structures fabricated using continuous fibre reinforced and the properties changes up to an order of magnitude by changing the fibre direction from parallel to perpendicular to the loading. Due to this anisotropic behaviour, AML can be used to find the desire pattern for each layer to improve mechanical properties [21]. Therefore, mechanical properties of 3D printed polymer composites with continuous carbon fibre were evaluated by testing five sample for each configuration (0°, 90°, ±45 and Quasi-isotropic) and was compared with the unreinforced samples. The numbers of carbon fibre layers were 24 for all configuration with top and bottom layer of nylon in order to easily remove the printed part from build platform.

From these test combinations values of modulus in longitudinal direction (E_1), transverse elastic modulus (E_2), shear modulus (G_{12}), poison's ratio (ϑ_{12}), longitudinal tensile strength (TS_1), transverse tensile strength (TS_2) and in-plane shear strength (τ_{12}) was obtained. Tensile testing of samples with fibers orientating at 0° yields E_1,ϑ_{12} and tensile strength in longitudinal direction. The longitudinal modulus is obtained from the initial portion of the stress strain curve in tensile testing using the relation $E_1 = \frac{\sigma_1}{\varepsilon_1}$, while the major poison's ratio is obtained as the transverse strain over the longitudinal strain by $\varepsilon_2 = -\vartheta_{12}\varepsilon_1$. Transverse tensile strength (TS_2) is the minimum stress obtained with 90° orientation of the fibre.

The highest strength for the dog bone shaped samples achieved was 524.66 MPa with 34% of carbon fibre contents in the direction of load which was much higher than 270.63 MPa of strength achieved with 48.72% of carbon contents as reported by Justu et al [22]. The tensile strength for 3D printed specimens with a volume fraction of 35% is higher than 310 MPa for Aluminium 6061T-6 as reported [23]. Also E_1, E_2, G_{12}, υ_{12}, TS_1 was compared to the values in the literature and it was found that all the values are higher in number except tensile strength [16,24] and are summarized in Table 3. According to the standard, the sample must include tabs at the end zones in order to avoid damage or the generation of stress concentration that may be produced due to gripping system. Glass tabs were bonded to both sides of the sample using Araldite adhesive. Prior to bonding both the tabs and the samples (gripping area) were roughen with different grades of silicon carbide paper to improve adhesion and avoid slipping during the test (Table 4).

Table 3
Experimentally determined values from tensile tests comparison with the literature.

Values	Experimentally determined	Literature reference [16]	Literature reference [24]
E_1	73.20 GPa	52 GPa	69.4 GPa
E_2	4.1 GPa	4 GPa	3.5 GPa
G_{12}	2.2 GPa	2 GPa	1.9 GPa
υ_{12}	0.33	0.33	0.41
TS_1	524.66 MPa	700 MPa	805.4 MPa
TS_2	121.3 MPa	48 MPa	17.9 MPa
τ_{12}	61 MPa	73 MPa	61.5 MPa

Table 4
Tensile strength, Young's modulus and Poison's ratio for different 3D printed composite specimens.

Test type	Property	Mean value	Standard Error
Zero-degree orientation tensile samples	TS_1	524.66 MPa	1.80
	E_1	73.20 GPa	1.41
	υ_{12}	0.33	0.01
Ninety-degree orientation tensile samples	TS_2	38.66 MPa	2.77
	E_2	4.1 GPa	0.17
	υ_{21}	0.19	0.02
Quasi-isotropic orientation tensile samples	TS	273.6 MPa	12.46
	E	50.83 GPa	1.13

3. Results and discussion

The tensile tests gave some predictable and some interesting results. The Isotropic fill type with maximum layers of carbon fibres had the highest strength compared to all other configuration. The strength of the fibre 90° orientation was much lower than the strength of the samples at 0° orientation. Premature failure was noticed for the 0° fibre orientation because of discontinuity and the fibres were not aligned perfectly as reported by [13,25]. Typical failure location (samples shoulder) for the samples with zero-degree fibre orientation was at the starting point of fibre placement that is transition between the neck and flange area of the sample. The printer start printing at position 1 and ends at position 2 and then at point 3 and 4 discretely as shown in Fig. 4. Fibre misalignment can yield up to 30% reduction in tensile strength. Initially, the failure occurs far from the gage length area and was closer to the load application point near the grips which may have stress concentration due to griping. The stress versus strain curve is approximately linear elastic which is a characteristics of continuous carbon fibre reinforced composites. From the experimental data it is obvious that the mechanical properties such as tensile strength and elastic modulus are affected by the fibre orientation significantly (Figs. 5–7).

Fibre breakage sound was heard during the test along with some inconsistency in the stress strain curve shown in Fig. 8 and then the load was transferred from one to the other fibre until complete failure occur. Failure occur due to stress concentration at the radiused corners that is between the neck and the flange area as same issue reported by Sung et al. [17]. This is due to the cut-off of fibre at such transition points. Local voids or defects can be another reason of the individual fibre breakage which also cause damage to the nearby fibre by increasing stress concentration. Failure in different specimens occurred due to fibre breakage, fibre pull out and delamination. For the samples with fibre in longitudinal direction breakage occur at the corner and thus failure occur near this point. Also, it was noticed from the experiments that the Young's modulus and tensile strength is strongly influenced by the fibre orientation with respect to the direction of the applied load. For the fibre with orientation from 0° to ±45° the composite become softer, easier to deform and so the elongation becomes larger. For specimens with 90° orientation the elongation of the specimens decreases.

Rule of mixture (ROM) can be applied to estimate the strength and stiffness of the 3D printed specimens prior to the manufacturing of a composite. ROM calculate the mechanical properties of the composite

Fig. 4. Tensile sample with zero degree of fibre orientation (Eiger slicing software).

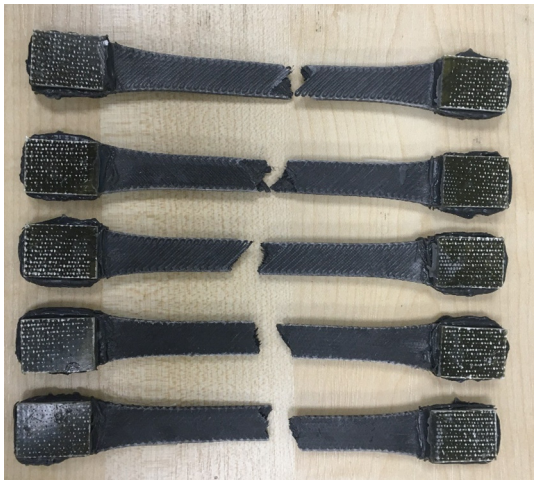

Fig. 5. Dog-bone shaped 3D printed composite specimens with glass tabs after failure.

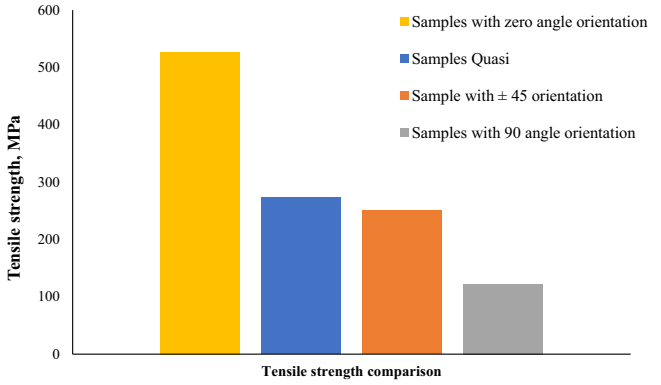

Fig. 6. Tensile strength comparison of composite specimens with different fibre angle orientation.

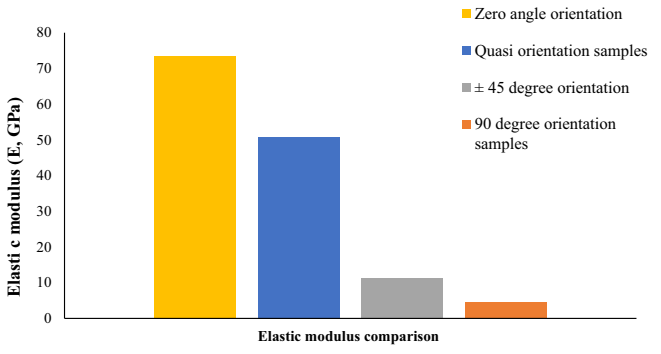

Fig. 7. Comparison of elastic modulus of composite specimens with different fibre angle orientation.

based on the individual properties of the matrix and the fibre. Fibre volume fraction of 34% was considered along with 3530 MPa of strength and 230 GPa of fibre stiffness for Toray carbon fibres to estimate upper limits using the following relation and it turn out to be 1200 MPa and 78 GPa respectively reported by Werken [16]. An upper limit of 1000 MPa was considered due to manufacturing defects, high voids contents and weak adhesion between the matrix and the fibre. Elastic modulus values obtained in this paper was in the range of ±7% with that of the above-mentioned work.

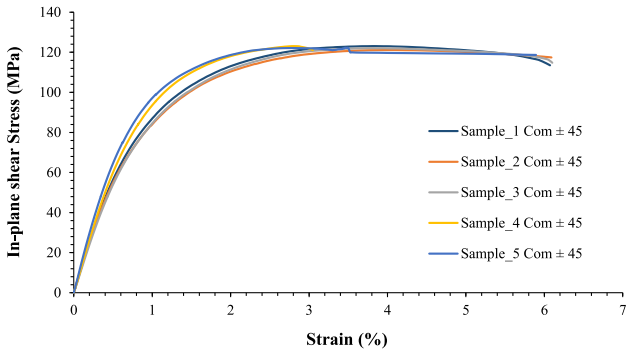

Fig. 8. Stress strain curve for 3D printed composite specimens with ±45-degree fibre orientation.

Tensile strength of the composite,

$$\sigma_c = \sigma_f V_f + \sigma_m V_m$$

Elastic modulus of the composite,

$$E_c = \eta E_f V_f + E_m V_m$$

However the prediction of elastic modulus is effective in the axial direction using ROM while it fails to predict the tensile strength accurately [26]. Furthermore, ROM assumes that the fibre is aligned unidirectionally with uniformly distributed stress. For the elastic modulus in the transverse direction, the following relation can be used;

$$\frac{1}{E_t} = \frac{V_m}{E_m} + \frac{V_f}{E_f}$$

3.1. In-plane shear properties

In-plane shear properties of composite specimens were determined by printing samples with ±45 alignment of the fibre alternatively according to ASTM D3518 standards. Strain in longitudinal and transverse direction were obtained from two extensometers and shear modulus was calculated from the graph between shear strength and shear strain. Shear stress was calculated the flowing relation $\tau = \frac{F}{2bh}$,while the in-plane shear modulus was calculated using$G_{12} = \frac{\tau_{12}}{\gamma_{12}}$. Shear modulus and shear stress values obtained was 2.2 GPa and 61 MPa respectively. The in-plane shear strength and shear modulus was 61.5 MPa and 1.9 GPa respectively in the literature reported by Iraqi et al. [24]. Stress strain curve for ±45 orientation samples are shown in Fig. 8.

3.2. Rectangular verses dog-bone shape comparison

Tensile tests on rectangular specimens were conducted according to ASTM D3039 standards as dog-bone shaped specimens have premature failure due to the discontinuity in the fibre placement at the corners. Three types of rectangular specimens i.e. Specimens bonded with glass tabs, specimens with printed tabs of pure nylon and specimens printed with carbon fibre tabs as shown in Fig. 9. It should be noted that in case of printed tabs support material was added during the manufacturing and was removed after printing finish. Also, there was no difference in strength and stiffness of the specimens printed with and without any support material. It took too long however, for

Fig. 9. Rectangular tensile samples with 3D printed and glass tabs with strain gages.

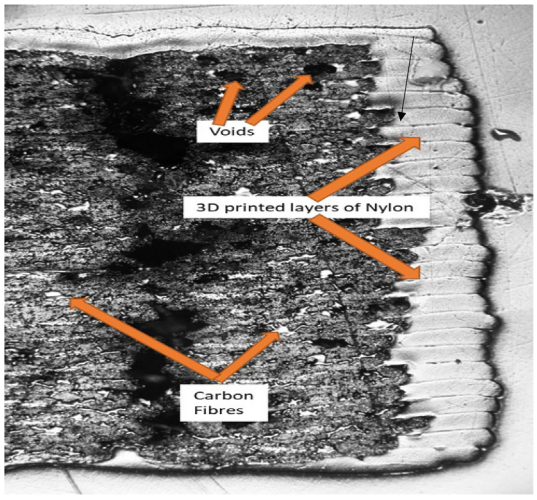

Fig. 10. Cross sectional micrographs of the 3D printed composite specimens showing horizontal lines the individual layer thickness along with porosity (voids) and fibre.

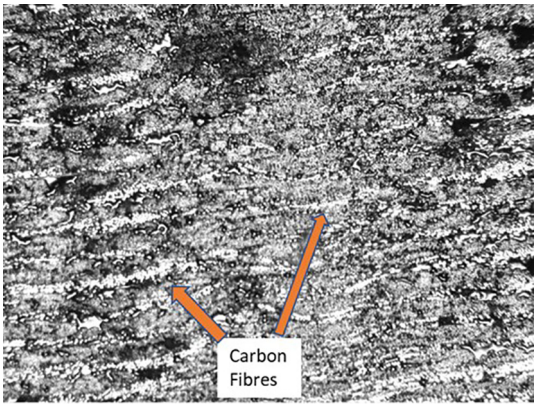

Fig. 11. Cross sectional image of the polished composite sample showing printed tracks along with the voids.

the tabs to manufacture along with the sample and a lot of material waste also happen just for obtaining the tabs. Strain gages were also mounted on the samples to measure the strain in longitudinal and transverse direction and was compared to the values obtained using extensometer. There was no difference between the values of Poison's ratio obtained using two different approaches. The highest tensile strength and elastic modulus achieved for rectangular samples were 603.43 MPa and 85 GPa respectively.

4. Optical microscopy

3D printed test samples used in this study were examined using an optical microscope in order to gain insights into the internal structure, voids formation and the bonding mechanism of the samples. Samples were clamped using a ring and mounted using cold cured epoxy resin in 30 mm diameter sample cup. Silicone oil was applied to the interior of the cups in order to remove the sample easily. Resin and hardener were mixed at a ratio of 15:2 and poured over the composite sample of the fibre reinforced 3D printed parts. The sample was cured at room temperature for 24 h. After curing, the samples were then prepared for microscopy by grinding using silicon carbide paper of different grades followed by polishing. Images of the samples were taken using a high-resolution camera mounted with an adjustable magnification lens. Optical images of the 3D printed were captured to inspect the porosity as well as the state of the dispersion within the polymer composites. Typical images taken at different magnification are presented in Fig. 10 in which individual layer can be seen on the right side.

The microstructure of the printed parts was analyzed to evaluate the quality of the material and the distribution of fibre and the matrix from the longitudinal axis. For this purpose, sample printed with uni-directional CCF/PA was examined by optical microscopy. Microscopic images of the cross section at different magnifications are shown in Fig. 11. The inter layer limits of the PA are visible near the edge of the sample. The presence of voids in large may indicate the printing process is unable to adequately compact the extruded filament on the printed part. From the figures, it can also be observed that the fibre distribution is non-uniform. Large matrix dominated and high fibre density zones can be clearly distinguish in Fig. 11.

5. Thermal analysis (Differential scanning calorimetry (DSC))

DSC analysis was done of the filament before and after printing using heat cool heat cycle to find the glass transition temperature, melting point and heat of reaction. About 8–10 mg of sample was heated from room temperature up to 300 °C at a rate of 10 °C/min and then cooled at the same rate and reheated again to remove the thermal history of the material. Fig. 12 show DSC result of the filament before printing and the printed sample. TGA equipment (Q 600, TA instruments) was used to evaluate the thermal behavior and the composition of the composite materials up to 600 °C in nitrogen atmosphere. Weight loss of 5–8% was observed up to 150 °C that might be due to evaporation of moisture contents. Degradation started at 400 °C and full decomposition was observed at around 520 °C. Melting (T_m), decomposition (T_d) and crystallization temperature (T_c) are summarized in Table 5 for filament before printing and for the printed part (Table 6).

6. Modelling approach using CLT for composites

Polymer fibre composites produced by FDM can be analysed using existing theories based on the manufacturing technique and the reinforcement type. Microstructure of 3D printed parts are often different from those prepared by traditional techniques, there is a demand for modelling and analysis of these 3D printed parts. Classical laminate theory (CLT) is also applicable for the 3D printed parts that are isotropic and homogeneous. Other assumptions include that each layer must

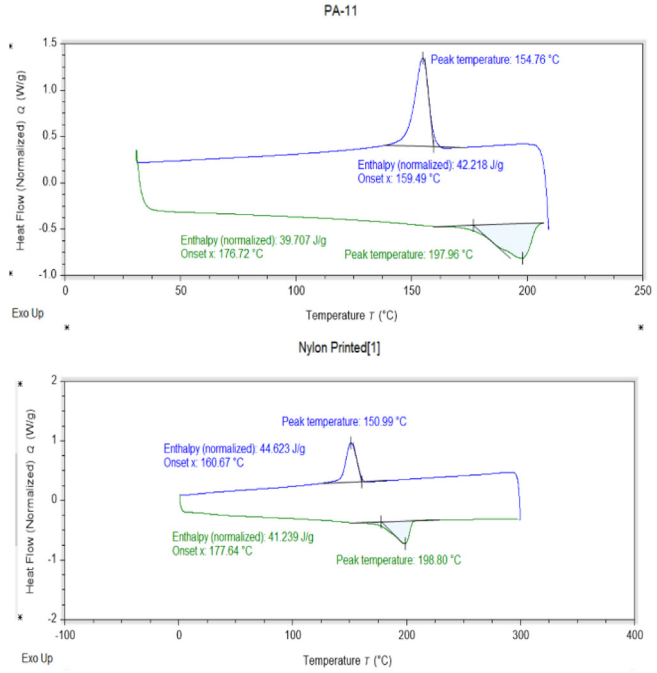

Fig. 12. DSC analysis of the PA filament and the printed samples to evaluate the effect of nozzle temperature on the polymeric material.

Table 5
Thermal properties of the nylon material before and after printing.

Material	T_m (°C)	T_c (°C)	T_d (°C)
PA filament	197.9 °C	37.6 °C	517.6 °C
PA Printed sample	198.8 °C	38.4 °C	520.3 °C

Table 6
3D printed composites layups configuration with their angle minus longitudinal.

Layup	AML
[0]s	−1
[90]s	0
[45,135]s	1
[0,45,135,90]s	0.25

be in a state of plane stress along with perfectly bonded layers. CLT allows the researcher to calculate the elastic behaviour of a multi-layer orthotropic material using the constants that describe the mechanical behaviour. Basic assumption are given in [27] and the stiffness matrix is defined as follow;

$$Q_{ij} = \begin{bmatrix} Q_{11} & Q_{12} & 0 \\ Q_{12} & Q_{22} & 0 \\ 0 & 0 & Q_{66} \end{bmatrix}$$

where

$$Q_{11} = \frac{{E_{11}}^2}{E_{11} - {\vartheta_{12}}^2 E_{22}}, Q_{12} = \frac{\vartheta_{12} E_{11} E_{22}}{E_{11} - {\vartheta_{12}}^2 E_{22}},$$

$$Q_{22} = \frac{E_{11} E_{22}}{E_{11} - {\vartheta_{12}}^2 E_{22}}, Q_{66} = G_{12}$$

Table 7
Comparison between the experimental and the predicted values determined using LAP.

Values	Experimental values	Predicted values using LAP
E_{11}	73.20 GPa	72.87 GPa
E_{22}	4.10 GPa	4.75 GPa
G_{12}	2.23 GPa	3.43 GPa
υ_{12}	0.33	0.31
τ_{12}	61 MPa	59 MPa

Transformed reduced stiffness matrix for various fibre orientation can be computed using transformation equation;

$$Q_{ij} = T^{-1} Q_{ij} T$$

where

$$T = \begin{bmatrix} m^2 & n^2 & 2mn \\ n^2 & m^2 & -2mn \\ -mn & mn & m^2 - n^2 \end{bmatrix}$$

In this equation m = cosθ, n = sinθ and θ is the angle fibre that is reinforced. In order to demonstrate the usefulness of employing CLT to model the FDM structures, the value of laminate Young's modulus will be compared with that measured experimentally.

AML values was calculated for each layup configuration to be used in analysis in LAP [28]. AML is the difference between the fibre contents percentage that are longitudinal to the principal loading direction. AML is the reference to indicate whether a layup is dominated by off plies angle or not. Four layups were chosen to analyse a range of sequence with each layup consists of 12 laminates having symmetry on the other side having a thickness of 0.125 mm.

The comparison between the experimental data and the results from LAP using CLT shows a great resemblance for Young's modulus in longitudinal direction. The difference between some of the predicted and the actual experimental values is due to the reasons of not taking some process parameters effects (compressive tensile strength and young's modulus) on 3D printed parts as they were not considered in the present work. Efficiency (Krenchel) factor of 0.375 must be applied for Quasi specimen. Poison's ratio calculated using LAP in transverse direction was 0.01853 which was the same as calculated using the relation $\upsilon_{21} = \upsilon_{12}\frac{E_2}{E_1}$[29]. Results from LAP was determined and compared with the experimentally determined values which are in good agreement with each other and are summarized in Table 7.

7. Conclusion

The main goal of this work was to study the effect of reinforcement on the mechanical properties of 3D printed polymer composites filled with continuous carbon fibres with different orientation that were produced using Mark Two printer. Maximum tensile strength and stiffness achieved for fibre in the loading direction was 524.66 MPa and 73 GPa and this was much higher than the unreinforced 3D printed parts (32 MPa and 0.84 GPa). Results showed that the mechanical properties obtained for 3D printed polymer composites are still not comparable to those obtained by traditional methods (pre-pegs). This may be due to fact that 3D printed structures have high level of porosity as well as low level of fibre contents. Furthermore, the improvement of the mechanical properties in comparison to unreinforced samples is significant. From the micrographs it was observed that the 3D printed composite parts exhibit a large amount of inhomogeneity having polymer rich and fibre rich regions. Strength and ductility of the specimen also depends on the amount and the orientation of the fibre contents. The predicted values for the quasi-isotropic specimens obtained using LAP show good agreement with the values obtained through experiments.

Declaration of Competing Interest

The authors declare that they have no known competing financial interests or personal relationships that could have appeared to influence the work reported in this paper.

Acknowledgements

The North West Centre for Advanced Manufacturing (NW CAM) project is supported by the European Union's INTERREG VA Programme, managed by the Special EU Programmes Body (SEUPB). The views and opinions in this document do not necessarily reflect those of the European Commission or the Special EU Programmes Body (SEUPB).

If you would like further information about NW CAM please contact the lead partner, Catalyst, for details."

References

[1] Tekinalp HL et al. Highly oriented carbon fiber–polymer composites via additive manufacturing. Compos Sci Technol 2014;105:144–50.
[2] Jia N, Fraenkel HA, Kagan VA. Effects of moisture conditioning methods on mechanical properties of injection Molded Nylon 6. J Reinf Plast Compos 2004;23(7):729–37.
[3] Wong KV, Hernandez A. A review of additive manufacturing. ISRN Mech Eng 2012;2012:1–10.
[4] Herbert N, Simpson D, Spence WD, Ion W. A preliminary investigation into the development of 3-D printing of prosthetic sockets. J Rehabil Res Dev 2005;42(2):141.
[5] Klammert U, Gbureck U, Vorndran E, Rödiger J, Meyer-Marcotty P, Kübler AC. 3D powder printed calcium phosphate implants for reconstruction of cranial and maxillofacial defects. J Cranio-Maxillofacial Surg 2010;38(8):565–70.
[6] Chua CK, Leong KF, Lim CS. Rapid prototyping: Principles and applications. third ed. World Scientific Publishing Co.; 2010.
[7] Mohamed OA, Masood SH, Bhowmik JL. Optimization of fused deposition modeling process parameters: a review of current research and future prospects. Adv Manuf 2015;3(1):42–53.
[8] Torrado Perez AR, Roberson DA, Wicker RB. Fracture Surface Analysis of 3D-Printed Tensile Specimens of Novel ABS-Based Materials. J Fail Anal Prev, Jun 2014;14(3):343–53.
[9] Biron M. Thermoplastics and Thermoplastic Composites. Second ed. Elsevier Ltd; 2012.
[10] Y. Peng, Y. Wu, K. Wang, G. Gao, and S. Ahzi, "Synergistic reinforcement of polyamide-based composites by combination of short and continuous carbon fibers via fused filament fabrication," Compos. Struct., vol. 207, no. August 2018, pp. 232–239, 2019.
[11] Ning F, Cong W, Hu Z, Huang K. Additive manufacturing of thermoplastic matrix composites using fused deposition modeling: a comparison of two reinforcements. J Compos Mater 2017;51(27):3733–42.
[12] Goh GD et al. Characterization of mechanical properties and fracture mode of additively manufactured carbon fiber and glass fiber reinforced thermoplastics. Mater Des 2018;137:79–89.
[13] Van Der Klift F, Koga Y, Todoroki A, Ueda M, Hirano Y, Matsuzaki R. 3D Printing of Continuous Carbon Fibre Reinforced Thermo-Plastic (CFRTP) Tensile Test Specimens. Open J Compos Mater 2016;06(01):18–27.
[14] Rodriguez JF, Thomas JP, Renaud JE. Characterization of the mesostructure of fused-deposition acrylonitrile-butadiene-styrene materials. Rapid Prototyp J 2000;6(3):175–85.
[15] "Metal and Carbon Fiber 3D Printers for Manufacturing | Markforged." [Online]. Available: https://markforged.com/. [Accessed: 04-Apr-2020].
[16] N. van de Werken, J. Hurley, P. Khanbolouki, A. N. Sarvestani, A. Y. Tamijani, and M. Tehrani, "Design considerations and modeling of fiber reinforced 3D printed parts," Compos. Part B Eng., vol. 160, no. April 2018, pp. 684–692, 2019.
[17] Ahn SH, Montero M, Odell D, Roundy S, Wright PK. Anisotropic material properties of fused deposition modeling ABS. Rapid Prototyp J 2002;8(4):248–57.
[18] "ASTM F2792 - 12a Standard Terminology for Additive Manufacturing Technologies, (Withdrawn 2015)." [Online]. Available: https://compass.astm.org/Standards/WITHDRAWN/F2792.htm. [Accessed: 13-May-2019].
[19] A. M. Forster, "Materials testing standards for additive manufacturing of polymer materials: State of the art and standards applicability," in Additive Manufacturing Materials: Standards, Testing and Applicability, Nova Science Publishers, Inc., 2015, pp. 67–123.
[20] Pascual-González C, Iragi M, Fernández A, Fernández-Blázquez JP, Aretxabaleta L, Lopes CS. An approach to analyse the factors behind the micromechanical response of 3D-printed composites. Compos Part B Eng 2020;186:107820.
[21] Hu Z et al. Design of ultra-lightweight and high-strength cellular structural composites inspired by biomimetics. Compos Part B Eng 2017;121:108–21.
[22] T. Yu, Z. Zhang, S. Song, Y. Bai, and D. Wu, "Tensile and flexural behaviors of additively manufactured continuous carbon fiber-reinforced polymer composites," Compos. Struct., vol. 225, no. June, 2019.
[23] "Aluminum 6061-T6; 6061-T651." [Online]. Available: http://www.matweb.com/search/datasheet.aspx?MatGUID=b8d536e0b9b54bd7b69e4124d8f1d20a&ckck=1. [Accessed: 22-Jun-2020].
[24] M. Iragi, C. Pascual-González, A. Esnaola, C. S. Lopes, and L. Aretxabaleta, "Ply and interlaminar behaviours of 3D printed continuous carbon fibre-reinforced thermoplastic laminates; effects of processing conditions and microstructure," Addit. Manuf., vol. 30, no. July, p. 100884, 2019.
[25] Justo J, Távara L, García-Guzmán L, París F. Characterization of 3D printed long fibre reinforced composites. Compos Struct 2018;185:537–48.
[26] "Amazon.com: An Introduction to Composite Materials (Cambridge Solid State Science Series) eBook: Hull, D., Clyne, T. W.: Kindle Store." [Online]. Available: https://www.amazon.com/Introduction-Composite-Materials-Cambridge-Science-ebook/dp/B00E3UR8K8. [Accessed: 30-Jun-2020].
[27] Introduction to Composite Materials Design, Third Edition. CRC Press, 2017.
[28] [Online]. Available: http://www.anaglyph.co.uk/lap.htm. [Accessed 27-May-2020].
[29] Casavola C. Orthotropic mechanical properties of fused deposition modelling parts described by classical laminate theory. Duke Law J 2019;1(1):1–13.